J. Chem. Sci. Vol. 127, No. 7, July 2015, pp. 1145–1153.
DOI 10.1007/s12039-015-0891-1

Tuning the structural and catalytic properties of ceria by doping with Zr^{4+}, La^{3+} and Eu^{3+} cations

T VINODKUMAR, D NAGA DURGASRI, SWAMY MALOTH and BENJARAM M REDDY*
Inorganic and Physical Chemistry Division, CSIR – Indian Institute of Chemical Technology, Uppal Road, Hyderabad 500 007, India
e-mail: bmreddy@iict.res.in; mreddyb@yahoo.com

MS received 31 December 2014; revised 27 March 2015; accepted 28 March 2015

Abstract. This work attempts to gain information about the role of trivalent and tetravalent dopants on the structural and catalytic properties of ceria (CeO_2). In this study, we have prepared Zr^{4+}, La^{3+}, and Eu^{3+} doped ceria (CZ, CL, and CE) by coprecipitation method and calcined at 773 K. The physicochemical characterization was achieved by using various techniques, namely, X-ray powder diffraction (XRD), Brunauer-Emmett-Teller (BET) surface area, high resolution transmission electron microscopy (HRTEM), Raman spectroscopy, temperature programmed reduction (TPR), X-ray photoelectron spectroscopy (XPS), and electron spin resonance (ESR) spectroscopy. The catalytic efficiency for soot oxidation was evaluated by thermogravimetric (TG) method and compared with undoped CeO_2. Doped CeO_2 catalysts decreased the soot oxidation temperature by more than 158 K compared to pure ceria. This is ascribed to mutual interaction and synergistic effect between the dopant species and the ceria. Among the synthesized nanocatalysts, the CE sample exhibited better performance. The observed better activity of CE was attributed to the presence of more number of oxygen vacancies, a high specific surface area, and easy reducibility as confirmed from Raman, BET surface area, and TPR measurements, respectively.

Keywords. Doped ceria; coprecipitation method; oxygen vacancies; soot oxidation

1. Introduction

In recent years, market share of diesel engines in the world has increased significantly owing to their superior fuel economy, low CO_2 emissions, and high durability in comparison with gasoline-powered vehicles.[1] However, pollution from diesel-powered vehicles contributes a significant amount of planetary air-quality problems due to the emission of soot particulates.[2–5] In general, particulate filters are used in engine exhaust pipelines to capture the soot particulates. However, the trapped soot accumulates in the diesel particulate filter (DPF) channels resulting in backpressure, which potentially decreases the engine efficiency.[6,7]

Alternatively, a combination of traps and oxidation catalysts appeared to be the most promising technology for soot elimination. The function of catalysts in this application is to reduce the soot ignition temperature and increase the oxidation rate of soot collected on the filter during trap regeneration. In the last decade, a large amount of work has been carried out on catalyst formulations. Different catalysts have been investigated for this purpose, which include noble metals, alkali metals, alkali earth metals, transition metals, and rare earth metals. Based on the laboratory results obtained by several research groups,[8–10] ceria-based catalysts have been proposed as promising materials because of their high oxygen storage and release capacity (OSC) which is represented in the following equation:

$$2CeO_2 \leftrightarrow Ce_2O_3 + {}^1/_2\, O_2 \qquad (1)$$

Each released O atom leaves a vacancy (Vö) and creates two Ce^{3+} ($Ce\ 4f^1$) cations by transferring electrons to two Ce^{4+} cations ($Ce\ 4f^0$). This property confers the ability to adsorb gaseous O_2 and form active oxygen at the catalyst surface (O_{ads}), which can be transferred to the soot–catalyst interface by superficial diffusion. The transfer of active oxygen from catalyst surface to the soot is the most important parameter in catalyzing the soot oxidation.[11,12] It is well-known that modification of ceria by doping with transition and rare earth metal cations induces several benefits on the catalytic features of ceria such as improvement in the thermal stability, enhanced surface reducibility, and high oxygen mobility, which contribute to the effective elimination of soot particles.[13–15]

Towards this end, nanosized CeO_2–ZrO_2(CZ), CeO_2–La_2O_3(CL), and CeO_2–Eu_2O_3(CE) catalysts are

*For correspondence

considered as the most promising candidates. Since, these foreign cations alone (Zr^{4+}, La^{3+}, and Eu^{3+}) are very active in various applications including oxidation reactions. Several authors reported that doping of Zr^{4+} into the ceria lattice enhances the catalytic performance by creating structural defects and increase the channel diameter for oxygen migration in the lattice.[16] On the other hand, doping of La^{3+} and Eu^{3+} into the ceria network improves the oxygen vacancies by decreasing the activation energy for oxygen vacancy formation.[17,18] These oxygen vacancies are the most decisive factors for catalyzing the soot oxidation. Therefore, by considering the aforesaid essential features of dopants, we were interested to investigate the CZ, CL, and CE catalysts for soot oxidation. Accordingly, the present work was undertaken with an aim to investigate how the dopants improve the catalytic properties of ceria by using various physicochemical techniques, namely, X-ray diffraction (XRD), BET surface area, high resolution transmission electron microscopy (HRTEM), Raman spectroscopy (RS), temperature programmed reduction (TPR), X-ray photoelectron spectroscopy (XPS), and electron spin resonance (ESR) spectroscopy. Synthesized catalysts were tested for soot combustion by TGA method under tight contact mode. The investigated materials were prepared by a modified coprecipitation method and a pure CeO_2 sample was also prepared under identical conditions for comparison purpose.

2. Experimental

2.1 *Catalyst preparation*

The investigated CeO_2–ZrO_2 (CZ 1:1 mole ratio), CeO_2–La_2O_3 (CL 8:2 mole ratio), and CeO_2–Eu_2O_3(CE 8:2 mole ratio) solid solutions and a reference CeO_2 were synthesized by a modified coprecipitation method using appropriate amounts of the corresponding Ce $(NO_3)_3{\cdot}6H_2O$ (Aldrich, AR grade), $ZrO(NO_3)_2{\cdot}xH_2O$ (Fluka, AR grade), $La(NO_3)_3{\cdot}6H_2O$ (Aldrich, AR grade), and $Eu(NO_3)_3{\cdot}5H_2O$ (Aldrich, AR grade) precursors respectively. The desired amounts of the precursors were dissolved separately in double-distilled water under mild stirring conditions and mixed together. Dilute aqueous ammonia solution was added drop-wise over a period until the pH of the solution reached ~8.5. The resulting pale yellow coloured slurry was decanted, filtered, and washed several times with double distilled water until free from anion impurities. The obtained precipitate was oven dried at 393 K for 12 h and calcined at 773 K for 5 h at a heating rate of 5 K min^{-1} in air atmosphere. For convenience CeO_2–ZrO_2, CeO_2–La_2O_3, CeO_2–Eu_2O_3, and CeO_2 are designated as CZ, CL, CE, and C, respectively.

2.2 *Catalyst characterization*

XRD data was acquired in the 2θ range of 12–80° on a Rigaku Multiflex instrument using Cu Kα ($\lambda = 1.5418$ Å) radiation and a scintillation counter detector. Crystalline phases present in the samples were identified with the help of Powder Diffraction File-International Centre for Diffraction Data (PDF-ICDD). The average size of the crystalline domains (D) of the prepared materials were estimated with the help of the Scherrer equation (2) using the XRD data of all prominent lines.

$$D = K\,\lambda/\beta\cos\theta \tag{2}$$

Where D denotes the crystallite size, λ the X-ray wavelength (1.541 Å), K the particle shape factor taken as 1, β the peak width (FWHM, full width at half maximum) in radians and θ the Bragg diffraction angle. The lattice parameter 'a' was calculated by a standard cubic indexation method using the intensity of the base peak (111). BET surface area measurements were made on a Micromeritics ASAP 2020 instrument. Prior to analysis, the samples were oven dried at 393 K for 12 h and flushed with argon gas for 2 h. The BET surface area was measured by nitrogen adsorption-desorption isotherms at liquid nitrogen temperature.

HRTEM studies were made on a JEM-2010 (JEOL) instrument equipped with a slow-scan CCD camera at an accelerating voltage of 200 kV.

Raman spectra were recorded with a Horiba Jobin Yvon HR 800 Raman spectrometer at ambient temperature. The emission line at 638.2 nm from the Ar^+ laser (Spectra Physics) was focused on the sample under the microscope.

Reducibility of the samples was examined by TPR using thermal conductivity detector of a gas chromatograph (Shimadzu) in a conventional apparatus. Approximately 30 mg of the sample weight was loaded in an isothermal zone of the reactor and heated at a rate of 10 K min^{-1} to 473 K using 30 mL min^{-1} He gas flow which facilitated to drive away the molecules that had been pre-adsorbed on the surface of the sample. After the sample was cooled to room temperature, the He was switched to 5% H_2/Ar with a rate of 20 mL min^{-1} and the temperature was linearly raised to 1073 K at a continuous heating ramp of 5 K min^{-1}, keeping all the parameters unchanged. The hydrogen consumption during the reduction process was calculated by passing the effluent gas through a molecular sieve trap to remove the produced water and was analyzed by gas chromatograph using TCD.

The XPS measurements were performed on a Shimadzu (ESCA 3400) spectrometer by using Al Kα (1486.7 eV) radiation as the excitation source. Charging effect of catalyst samples were corrected by using the binding energy of the adventitious carbon (C 1s) at 284.6 eV as internal reference. The XPS analysis was done at ambient temperature and pressures usually in the order of less than 10^{-8} Pa.

The electron paramagnetic resonance (EPR) measurements were carried out at room temperature with a Bruker EMX spectrometer operating in the X band. The spectra were calibrated with a standard diphenylpicrylhydrazyl (DPPH) (g = 2.0036).

2.3 *Catalyst evaluation*

The catalyzed soot oxidation was studied in a thermogravimetric analyzer (Mettler Toledo, TGA/SDTA851e). Oxidation experiments consisted of heating the soot–catalyst mixtures at 10 K min^{-1} from 100 to 1273 K in 100 mL min^{-1} flow of air. These experiments were conducted in 4–5 cycles using the same catalyst sample. No appreciable change in the soot oxidation activity was noticed. The activity measurements were performed in 'tight contact' (ground in an agate mortar) condition with catalyst–soot mixtures in 4:1 wt/wt ratio. The model soot used is Printex-U provided by Degussa.[10] This soot has proven to be an appropriate model for the soot oxidation reaction.

3. Results and Discussion

3.1 *Characterization studies of the solid solutions*

Figure 1a presents the XRD patterns of CZ, CL, and CE samples along with pure ceria calcined at 773 K. As can be noted from the figure, all diffraction patterns could be indexed to ceria fluorite structure. Interestingly, the characteristics peaks corresponding to ZrO_2 or La_2O_3 or Eu_2O_3 phases are not visible in the investigated range. From figure 1b, it is clear that the diffraction peaks of the doped ceria are shifted with respect to pure ceria, confirming the formation of solid solutions. Lattice parameter values of CZ, CL, and CE samples (Table 1) are calculated by using the most intense base peak, and these values are found to vary from the bare ceria. This is primarily due to the doping of Ce^{4+} (0.97 Å) with smaller radius Zr^{4+} (0.84 Å) cations which leads to the shrinkage of the lattice (decreased lattice parameter). In the case of La^{3+} (1.10 Å) and Eu^{3+} (1.06 Å) whose ionic radius is larger than ceria, correspondingly their lattice parameters are increased. It

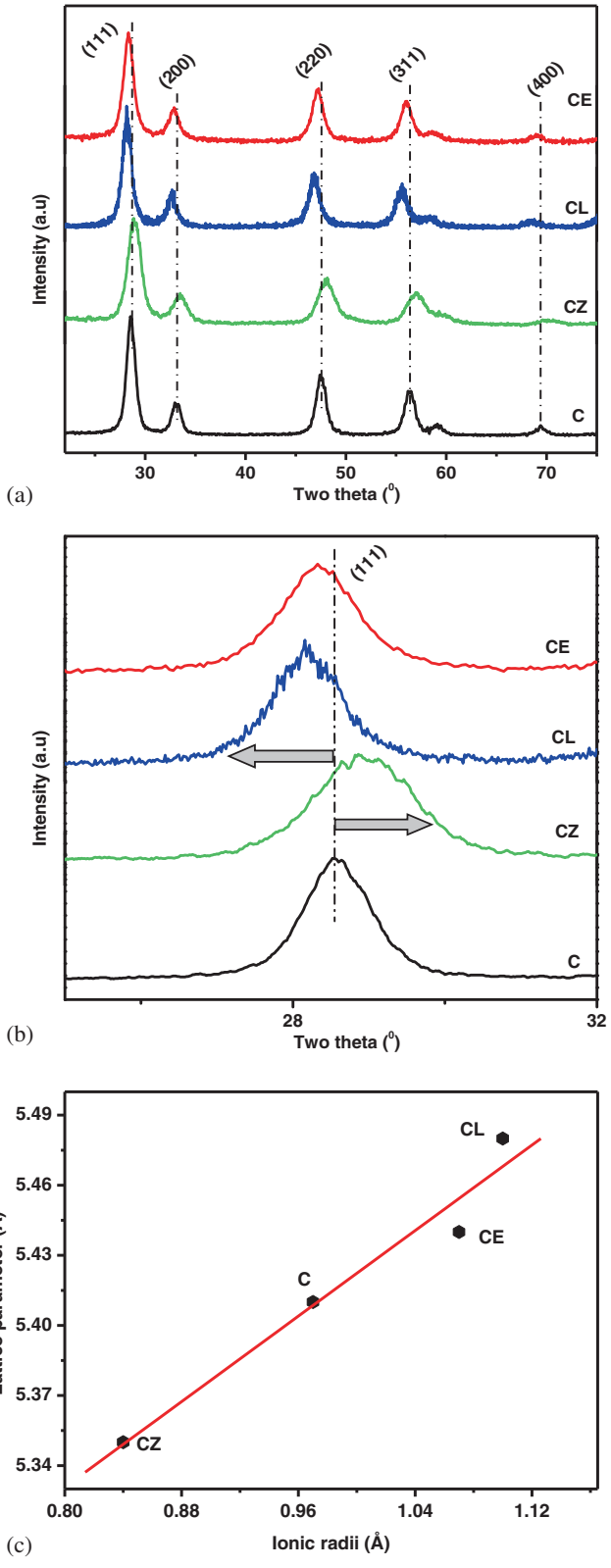

Figure 1. (a) Powder X-ray diffraction patterns of pure ceria (C), ceria–zirconia (CZ), ceria–lanthana (CL), and ceria–europia (CE) calcined at 773 K; (b) Enlarged X-ray diffraction patterns (2θ = 25-32°) of pure ceria (C), ceria–zirconia (CZ), ceria–lanthana (CL), and ceria–europia (CE) calcined at 773 K; (c) Lattice parameter versus ionic radii of the employed dopant cation.

confirms that lattice parameter strongly depends on the dopant size as shown in figure 1c. The changes in the lattice parameter values represent the distorted structure of ceria due to the substitution of dopants, which results easy annihilation of oxygen atoms in the lattice and could promote the soot oxidation. The mean crystallite size values of the synthesized materials are calculated by using the most prominent peaks such as (111), (220), and (311) with the help of Scherer equation and presented in table 1. From the figure 1a, it is apparent that all the reflections of doped ceria are less intense and broader. It indicates that the crystallite sizes of doped ceria are smaller than pure ceria. These values are in line with the particle size measured from the TEM analysis that is discussed in the later section. Besides these values, surface area calculated from the N_2 adsorption-desorption isotherms is also listed in table 1. From table 1, it is obvious that CZ, CL, and CE exhibit reasonably high specific surface area than pure ceria. Especially, the CE catalyst exhibited a high surface area than other samples, which signifies that addition of europium enhances the surface area of the ceria from 41 to 91 m^2/g.[19]

Table 1. Average crystallite size (D), lattice parameter '*a*', and BET surface area of pure ceria (C), ceria–zirconia (CZ), ceria-lanthana (CL), and ceria-europia (CE) calcined at 773 K.

Catalysts	C-773	CZ-773	CL-773	CE-773
Crystallite size (nm)	8.9	4.7	8.3	8.5
Lattice parameter (Å)	5.41	5.35	5.48	5.44
Surface area (m^2 g^{-1})	41	84	66	91

The HRTEM measurements were carried out on the CZ, CL, and CE samples calcined at 773 K and presented in figure 2. Analysis of these figures revealed that the average particle sizes of the prepared samples are in the range of 4–10 nm, which are in agreement with the XRD results. Furthermore, the materials exhibited well defined lattice fringes with a d spacing of about 0.307 to 0.309 nm which can be assigned to the (111) plane of the cubic CeO_2 structure.

Raman spectra of the synthesized samples are presented in figure 3a. Raman spectroscopy provides the information about the M-O bond arrangements and lattice defects. The Raman spectra of pure ceria displayed

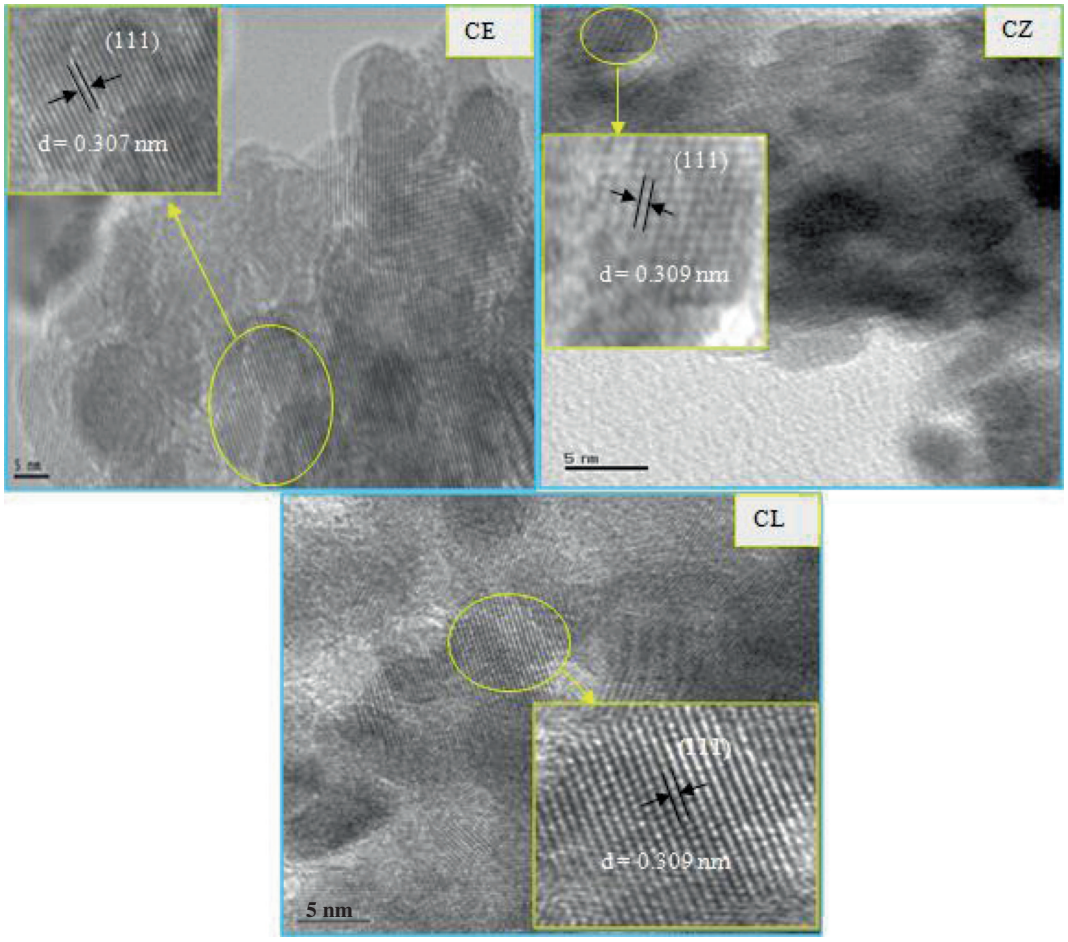

Figure 2. HRTEM images of ceria–zirconia (CZ), ceria–lanthana (CL), and ceria–europia (CE) calcined at 773 K.

a dominant peak at 464 cm^{-1} (F_{2g}). This band is related to the oxygen positions around cerium ions and is sensitive to the crystal symmetry. Along with this band, one more band observed at 600 cm^{-1}, which is due to the presence of CeO_8 complex (intrinsic oxygen defect). The slight shift in the Raman frequency and absence of peaks corresponding to ZrO_2 (t-ZrO_2; 268cm^{-1}, m-ZrO_2; 180cm^{-1}), La_2O_3 (405 cm^{-1}), and Eu_2O_3 (610 cm^{-1}) evidence the formation of solid solutions as indicated by XRD results.[20,21] Compared to pure ceria, the modified ceria with different dopants exhibit a significant difference in the spectra. In the case of pure ceria, the strongest peak centred at 464 cm^{-1} shifted by ~11 cm^{-1} towards higher wavenumber with Zr^{4+} dopant, and ~16 and ~6 cm^{-1} towards lower wavenumber with La^{3+} and Eu^{3+} dopants, respectively. As can be noted from figure 3(b), where the Raman shift (F_{2g} mode) is depicted as a function of experimental cell

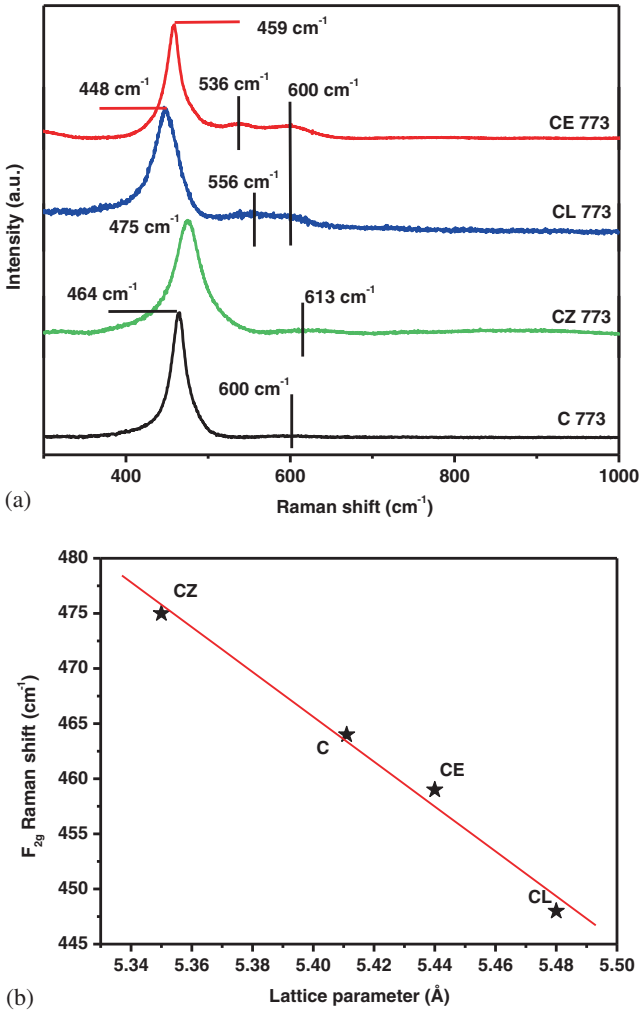

Figure 3. (a) Raman spectra of pure ceria (C), ceria–zirconia (CZ), ceria–lanthana (CL), and ceria–europia (CE) calcined at 773 K; (b) F_{2g} Raman mode shift versus lattice parameter of the prepared solids at 773 K.

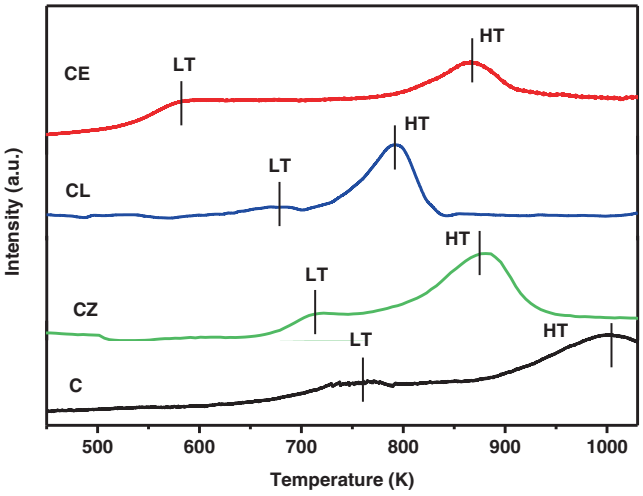

Figure 4. H_2 consumption curves of pure ceria (C), ceria–zirconia (CZ), ceria–lanthana (CL), and ceria–europia (CE) calcined at 773 K.

parameter determined from XRD results. Raman mode shifts downwards as the cell parameter increases and vice-versa. The observed general trend agrees with the expected Raman shift due to cell volume changes.[22]

Besides the strongest peak, one more band observed for Zr^{4+} doped ceria at 613 cm^{-1} and two peaks observed for La^{3+} and Eu^{3+} doped ceria between ~530–600 cm^{-1}. The former one is due to the presence of ZrO_8 type complex and can be termed as intrinsic oxygen defect. In the latter case, the peaks are due to the presence of both MO_8 type complex (M = La and Eu) and oxygen vacancies (extrinsic oxygen vacancies). The extrinsic oxygen vacancies are introduced in the ceria lattice by the substitution of trivalent dopant (La^{3+} and Eu^{3+}) with tetravalent cerium ions to compensate the effective negative charge.[23,24] From the Raman results, it can be stated that the existence of oxygen vacancies is more in trivalent doped ceria than tetravalent doped ceria. Among the prepared materials, the intensity of the Raman band in between 500–600 cm^{-1} is more for Eu^{3+} doped ceria in comparison to La^{3+} doped ceria material. In other words, qualitatively higher concentration of oxygen vacancies are detected in the Eu^{3+} doped ceria.[25] It implies that the mobility of oxygen ions via oxygen vacancies occurs readily in the Eu^{3+} doped ceria. These results are in a good agreement with the H_2-TPR results discussed in the following section.

The oxidation of ceria is much faster than its reduction and the promotion of reducibility in ceria is quite challenging due to its sluggish rate at which it is reduced. Therefore, any modification in the ceria by doping foreign cations induces more amount of oxygen vacancies that will improve the diffusion of oxygen

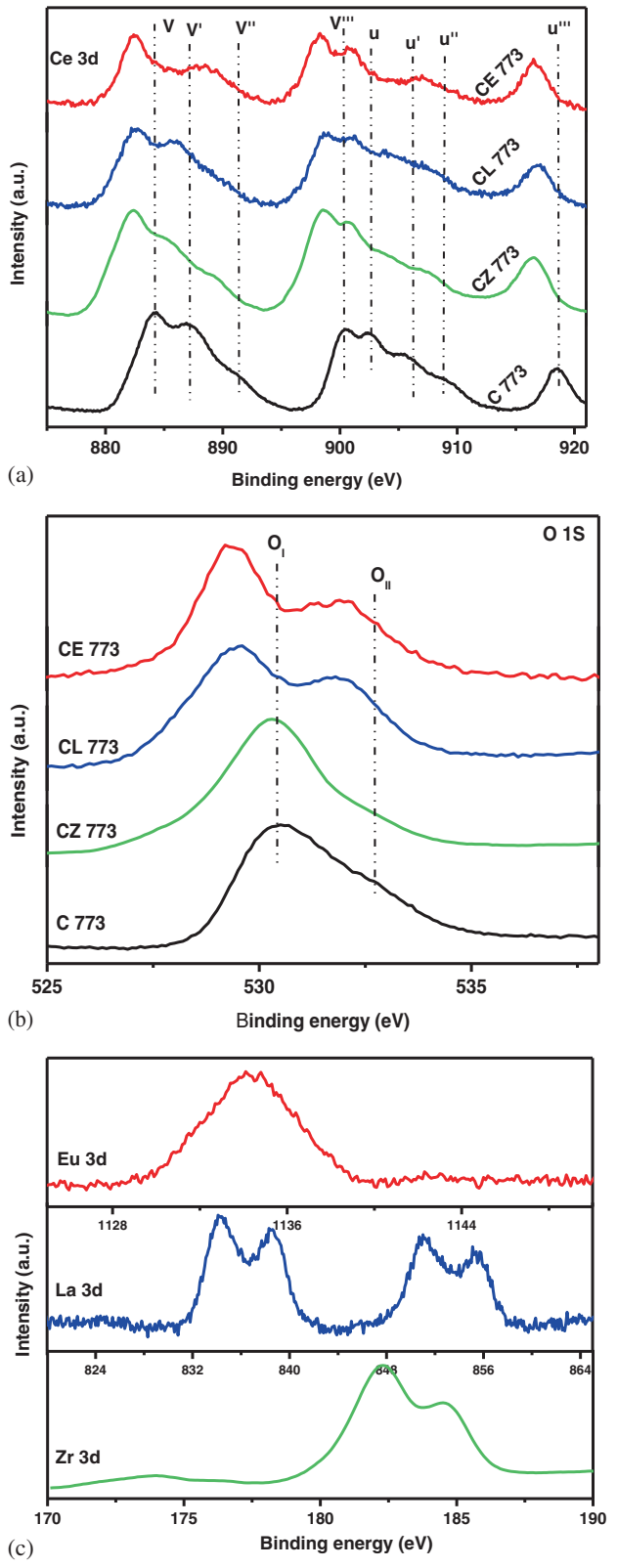

Figure 5. (a) Ce 3d XP spectra of pure ceria (C), ceria–zirconia (CZ), ceria–lanthana (CL), and ceria–europia (CE) calcined at 773 K; (b) O 1s XP spectra of pure ceria (C), ceria–zirconia (CZ), ceria–lanthana (CL), and ceria–europia (CE) calcined at 773 K; (c) Zr 3d, La 3d, and Eu 3d XP spectra of ceria–zirconia (CZ), ceria–lanthana (CL) and ceria–europia (CE) calcined at 773 K.

anions thereby increases the reducibility of ceria.[11] Effect of dopant on the reducibility of ceria is examined by temperature programmed reduction (TPR) under ambient conditions. The TPR profiles of doped ceria along with the pure ceria are shown in figure 4. It is important to note that under these experimental conditions the Ce^{4+} cations can only be reduced to Ce^{3+} but neither Zr^{4+} nor La^{3+} and Eu^{3+}. Therefore, the change observed among the H_2-reduction profiles of the doped ceria must be attributed to the effect of dopants.[26] Pure ceria undergoes two types of reductions at ~760 K and ~102 K. The former represents the surface reduction (LT) and the latter one due to bulk reduction (HT). During the surface reduction, the oxygen atoms are removed from the ceria surface and generate oxygen vacancies, these vacancies migrate from the surface to the bulk while the oxygen atoms move in the opposite direction. Upon doping with Zr^{4+} or La^{3+} or Eu^{3+} the amount of defects increased (according to the Raman results) and the oxygen mobility in the lattice enhanced, which facilitates the ceria reduction process at lower temperatures and is evident from the figure. Compared to CZ, the two reduction peaks (surface and bulk) of CL and CE are shifted to lower temperatures. This should be ascribed to the increased amount of oxygen vacancies due to the incorporation of trivalent cations into the ceria matrix in contrast to tetravalent substitution. With the increase of oxygen vacancies, oxygen mobility crossed a threshold limit and then materials are rapidly reduced[27,28] Compared to bare ceria the bulk reduction peaks of CZ, CL, and CE samples appeared at lower temperatures. It suggests that these dopants also facilitate the bulk Ce^{4+} reduction easily.[29]

XPS analysis was carried out in order to investigate the surface nature of the prepared materials. The XP spectra of Ce 3d core level for these samples are shown in figure 5a. In the Ce 3d spectra, the peaks labelled as u and v refers to the $3d_{3/2}$ and $3d_{5/2}$ spin–orbit components, respectively. In order to identify the specific oxidation state of cerium ions i.e., Ce^{4+} and Ce^{3+}, we labelled the spectra of Ce 3d and shown in figure 5a. As can be noted from the figure, the peaks designated as u, u″, u‴ and v, v″, v‴ can be assigned to Ce^{4+} while the peaks u′ and v′ belong to Ce^{3+} suggesting the coexistence of Ce^{3+} and Ce^{4+} in all the prepared materials. In all samples, the difference in binding energy of Ce $3d_{3/2}$ and Ce $3d_{5/2}$ (i.e. between u and v, u′ and v′, u″ and v″, and u‴ and v‴) varied between 18.5-19.5 eV in comparison to the standard expected value of 18.6 eV. This is in good agreement with the literature.[30] From the figure, it is apparent that the position of Ce 3d peaks shifted to lower binding energy compared to pure ceria indicating

the formation of vacancy defects in the doped samples in contrast to pure ceria.

O 1s spectra of prepared materials calcined at 773 K are presented in figure 5b. In the figure two peaks are observed, one is at 529.3–530.3 eV and other one is at 532.1–532.7 eV. The former one is related to the lattice oxygen (O_I) and the latter belongs to adsorbed oxygen (O_{II}). A keen observation of the figure reveals that the binding energy of O_I and O_{II} of doped ceria is lower than the pure ceria. It signifies that the environment present around the oxygen atoms is different i.e., Ce-O-Ce verses Ce-O-M (M = Zr, La, and Eu), which influence the properties of ceria significantly.[31]

Zr, La, and Eu 3d XP spectra of the prepared materials are shown in figure 5c. The Zr 3d photoelectron peaks were observed at 182.4 and 184.7 eV corresponding to Zr $3d_{5/2}$ and Zr $3d_{3/2}$ respectively, which are assigned to +4 oxidation state of the zirconium. The splitting energy difference between Zr $3d_{3/2}$ and Zr $3d_{5/2}$ photoemission feature is ~2.4 eV, which is in agreement with the earlier reports.[32] As for La species, the binding energy of La $3d_{5/2}$ in the calcined catalyst was about 834.91 eV indicating that La existed as La^{3+} species.[33] For XP spectrum of the Eu $3d_{5/2}$ binding energy, the peak observed at 1134 eV corresponds to Eu^{3+} and shows that the dopant present in the trivalent state only.[34]

The ESR spectra of CZ, CL, CE, and C are presented in figure 6. Among the prepared materials, only CZ is ESR active due to the presence of Ce^{3+}, which is paramagnetic in nature. From the figure, it is clear that the observed CZ spectrum is due to a superposition of two species with axially symmetric g-tensors and it shows two types of peaks designated as A and B. Peak A

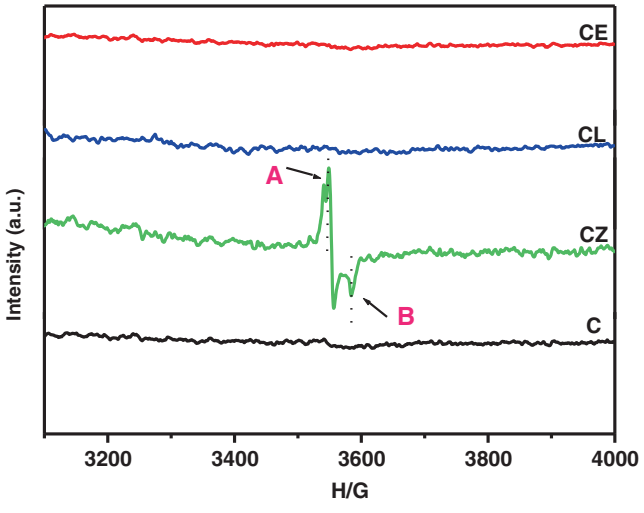

Figure 6. ESR spectra of pure ceria (C), ceria–zirconia (CZ), ceria–lanthana (CL), and ceria–europia (CE) calcined at 773 K.

(g = 1.940–1.942) corresponds to Ce^{3+} in terms of surface and peak B (g = 1.910–1.914) corresponds to Ce^{3+} in the bulk. No signal of oxygen vacancies like O^{2-} and O are detected due to low relaxation spin time at room temperature.[35–37] From XPS and ESR studies, it is clear that La and Eu are present in 3+ state, Zr in 4+ state, and Ce in 3+ and 4+ states respectively.

3.2 *Catalytic activity studies*

Normally diesel engines work under O_2 rich conditions (fuel lean condition). In this environment, ceria is able to exchange its oxygen with gas-phase oxygen. During this process highly active oxygen species (reactive oxygen species) are generated which can oxidize the soot very efficiently.[38] According to Trovarelli *et al*.[39] the mechanism of soot oxidation over ceria-based oxides is as follows:

$$Ce^{3+} - + \text{Gas-O} \rightarrow Ce^{4+} - (O - O)^{-} \quad (3)$$

$$Ce^{4+} - (O - O)^{-} + Cf \rightarrow Ce^{3+} + SOC \quad (4)$$

$$SOC \rightarrow CO \text{ or } CO_2 \quad (5)$$

Where Gas-O indicates the oxidant gas (O_2, NO, NO_2 etc.), Cf the carbon (soot) active site on the carbon surface and SOC a surface carbon–oxygen complex. In the first step, reduced ceria captures oxygen from the gas-phase molecules and is itself oxidizes by electron transfer from the Ce^{3+} surface to the adsorbed oxygen. In the second step, the oxygen of the oxidized ceria is transferred to an active site on the carbon surface and the ceria is reduced. In the third step, the formed SOC decomposes to yield CO or CO_2.[40] Among all the three steps, the second step is important, that is the transfer of oxygen from the catalyst to the soot surface and these transferred oxygens are called as active oxygens. The formation of these active oxygens and transfer depends on a number of parameters importantly on the oxygen vacancies (i.e., defect centres). The oxygen vacancy promotes the activation of adsorbed oxygen to form superoxides in the lattice. These types of oxygen react with soot efficiently. Very recently, Bueno-López has done TAP (temporal analysis of products) experiments and proved that soot is oxidized by participation of catalysts oxygen only i.e., lattice oxygen.[38] The catalytic conversion of soot (Printex U) as a function of temperature over pure ceria and doped ceria along with the uncatalyzed soot is compiled in figure 7. The catalytic activity could be evaluated by $T_{10,}T_{50,}$ and T_{90} values, which are defined as the temperatures at which 10%,

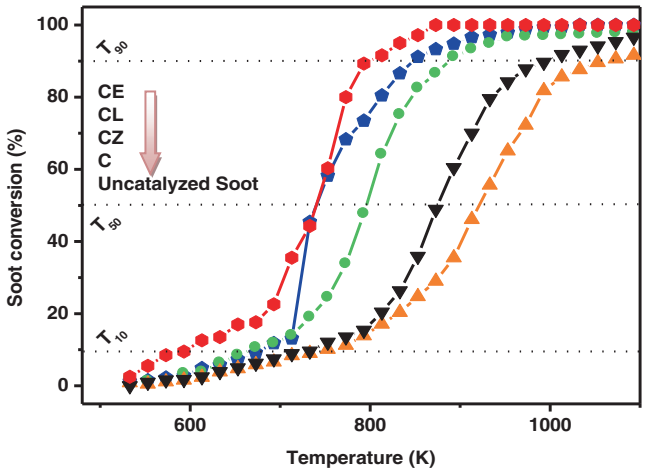

Figure 7. Normalized soot conversion (%) versus reaction temperature (K) of ceria (C), ceria–zirconia (CZ), ceria–lanthana (CL), and ceria–europia (CE) calcined at 773 K along with the uncatalyzed soot.

50% and 90% conversion of soot occurred (figure 8). The results indicate that europium-doped ceria exhibited better activity among all the materials. The temperature for T_{10} over all the catalysts is as follows: CE > CL > CZ > C > uncatalyzed soot; and the temperature difference between catalyzed soot and uncatalyzed soot is maximum ~158 K. For pure ceria and doped ceria the minimum and maximum temperature difference in the investigated materials is ~55 and 144 K. From this, it is apparent that the activity trend towards the soot combustion is as follows: doped ceria >pure ceria >uncatalyzed soot. In the case of T_{50} and $T_{90,}$ also we observed a similar trend. At 742 K, doped ceria shows maximum 50% and minimum 25% conversion but pure ceria shows only 15% conversion. The parameters that account for the difference in the activity include the specific surface area, presence of oxygen defects, and low temperature

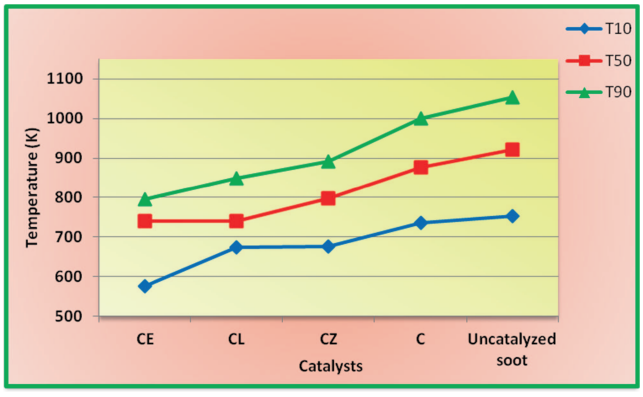

Figure 8. T_{10}, $T_{50,}$ and T_{90} of uncatalyzed soot, ceria (C), ceria–zirconia (CZ), ceria–lanthana CL), and ceria–europia (CE) calcined at 773 K.

surface reduction. As mentioned in the mechanism the supply of active oxygens are very important for soot oxidation. In the present case with the absence of catalyst, soot only starts to oxidize at above 600 K and slowly increases with oxidant gas. In the presence of catalyst (ceria), the activity is improved. Between the tetravalent (Zr^{4+}) and trivalent (Eu^{3+} and La^{3+}) dopants, the trivalent dopants improved ceria activity much better than tetravalent dopant. Since, the former dopants generate more oxygen vacancies, which induce more number of active oxygens than the later (confirmed from Raman and TPR results). Even though, La and Eu dopants are in the 3+ oxidation states the activity is more for Eu dopant only. A possible reason for this result might be that Eu^{3+} present in CE catalysts enhances the specific surface area, which provide more interface for soot to be in contact with the CE catalyst and other one is the availability of surface oxygen at low temperature as confirmed from TPR results. Compared to all other materials, CE catalyst generated more active oxygens, which are extremely reactive in the oxidation reactions.[41]

4. Conclusions

This work summarizes a complete structural and catalytic activity trends over various doped ceria materials. Tetravalent (Zr^{4+}) and trivalent (La^{3+}, Eu^{3+}) doped ceria materials were prepared by simple coprecipitation method and characterized by XRD, BET, TEM, Raman, TPR, XPS, and ESR techniques in order to understand the structural relationship with the catalytic activity. The obtained information for these samples is summarized as follows:

(i) Doped ceria materials are more suitable than pure ceria for soot oxidation. This is due to the improvement in the specific surface area, oxygen defects, and redox properties as confirmed from the BET, Raman, and TPR measurements.

(ii) Trivalent doped ceria (CL and CE) materials are more active than corresponding tetravalent doped ceria (CZ) for soot oxidation in the presence of air under tight contact condition.

(iii) Between CL and CE materials, the CE is more active towards soot combustion than CL. It could be due to the presence of more surface area, increased oxygen vacancies, and facile low temperature surface reduction. The overall soot oxidation efficiency on various samples is as follows: CE > CL > CZ > C > uncatalyzed soot; and the activity trend can be simply represented as doped ceria >pure ceria >uncatalyzed soot.

Acknowledgements

TV and DND thank the Council of Scientific and Industrial Research (CSIR), New Delhi for the research fellowships. SM thanks Department of Science and Technology (DST) New Delhi for financial support under SERB Scheme (SB/FT/CS-004/2013). Financial support for this project was received from Department of Science and Technology, New Delhi, under SERB Scheme (SB/S1/PC-106/2012).

References

1. Yamazaki K, Kayama T, Dong F and Shinjoh H 2011 *J. Catal.* **282** 289
2. Bensaid S, Russo N and Fino D 2013 *Catal. Today* **216** 57
3. Frank B, Schuster M E, Schlögl R and Su D S 2013 *Angew. Chem. Int. Ed.* **52** 2673
4. Yu Y, Meng M and Dai F 2013 *Nanoscale* **5** 904
5. Wen D 2010 *Energy Environ. Sci.* **3** 591
6. Raj A, Yang S Y, Cha D, Tayouo R and Chung S H 2013 *Combust. Flame* **160** 1812
7. Wagloehnera S, Baerb J N and Kuretia S 2014 *Appl. Catal. B Environ.* **147** 1000
8. Bharali P, Saikia P and Reddy B M 2012 *Catal. Sci. Technol.* **2** 931
9. Reddy L H, Reddy G K, Devaiah D and Reddy B M 2012 *Appl. Catal. A Gen.* **445–446** 297
10. Hernández-Giménez A M, Lozano-Castelló D and Bueno-López A 2014 *Appl. Catal. B Environ.* **148–149** 406
11. Esch F, Fabris S, Zhou L, Montini T, Africh C, Fornasiero P, Comelli G and Rosei R 2005 *Science* **309** 752
12. Meher S K and Rao G R 2012 *J. Colloid. Interface Sci.* **373** 46
13. Durgasri D N, Vinodkumar T, Sudarsanam P and Reddy B M 2014 *Catal. Lett.* **144** 971
14. Pradhan G K and Parida K M 2010 *Int. J. Eng. Sci. Tech.* **2** 53
15. Durgasri D N, Vinodkumar T and Reddy B M 2014 *J. Chem. Sci.* **126** 429
16. Hari Prasad D, Park S Y, Ji H -I, Kim H -R, Son J -W, Kim B -K, Lee H -W and Lee J -H 2012 *J. Phys. Chem. C* **116** 3467
17. Reddy B M, Katta L and Thrimurthulu G 2010 *Chem. Mater.* **22** 467
18. Vinodkumar T, Durgasri D N, Reddy B M and Alxneit I 2014 *Catal. Lett.* **144** 2033
19. Reddy B M and Rao K N 2009 *Catal. Commun.* **10** 1350
20. Escribano V S, Lopez E F, Panizza M, Resini C, Amores J M G and Busca G 2003 *Solid State Sci.* **5** 1369
21. O'Neill W M and Morris M A 1999 *Chem. Phys. Lett.* **305** 389
22. McBride J R, Hass K C, Poindexter B D and Weber W H 1994 *J. Appl. Phys.* **76** 2435
23. Li L, Chen F, Lu J -Q and Luo M -F 2011 *J. Phys. Chem. A* **115** 7972
24. Wei Y, Liu J, Zhao Z, Duan A and Jiang G 2012 *J. Catal.* **287** 13
25. Hernández W Y, Laguna O H, Centeno M A and Odriozola J A 2011 *J. Solid State Chem.* **184** 3014
26. Hernández-Giménez A M, dos Santos Xavier L P and Bueno-López A 2013 *Appl. Catal. A Gen.* **462–463** 100
27. Yao X, Tang C, Ji Z, Dai Y, Cao Y, Gao F, Dong L and Chen Y 2013 *Catal. Sci. Technol.* **3** 688
28. Wang N, Chua W, Zhang T and Zhao X -S 2011 *Chem. Eng. J.* **170** 457
29. Liu W, Feng L, Zhang C, Yang H, Guo J, Liu X, Zhang X and Yang Y 2013 *J. Mater. Chem. A* **1** 6942
30. Normand F L, Fallah J E, Hilaire L, Legare P, Kotani A and Parlebas J C 1989 *Solid State Commun.* **71** 885
31. Wang Z, Wang Q, Liao Y, Shen G, Gong X, Han N, Liu H and Chen Y 2011 *ChemPhysChem* **12** 1
32. Kanattukara V B, Dong-Kyu K and Dae-Won P 2010 *Nanoscale* **2** 1222
33. Wagner C D, Riggs W M, Davis L E and Moulder J F 1978 In *Handbook of X-ray photoelectron spectroscopy* (Eden Praire: Perkin-Elmer Corporation)
34. Kumar A, Babu S, Karakoti A S, Schulte A and Seal S 2009 *Langmuir* **25** 10998
35. Zhao M, Shen M, Weg X and Wang J 2008 *J. Alloys Compd.* **457** 578
36. Zhao M, Shen M and Wang J 2007 *J. Catal.* **248** 258
37. Wang J, Wen J and Shen M 2008 *J. Phys. Chem. C* **112** 5113
38. Bueno-López A 2014 *Appl. Catal. B Environ.* **146** 1
39. Aneggia E, de Leitenburga C, Llorcab J and Trovarelli A 2012 *Catal. Today* **197** 119
40. Bueno-López A, Krishna K, Makkee M and Moulijn J A 2005 *J. Catal.* **230** 237
41. Aneggi E, de Leitenburg C, Dolcetti G and Trovarelli A 2006 *Catal. Today* **114** 40